IJST, Transactions of Electrical Engineering, Vol. 36, No. E2, pp 189-206
Printed in The Islamic Republic of Iran, 2012

SELECTION THE BEST CONTROL CHANNEL FOR SSSC STABILIZER TO DAMP INTER-AREA OSCILLATION CONSIDERING NON-LINEARITY EFFECTS*

M. R. SHAKARAMI[1], A. KAZEMI[2] AND M. GITIZADEH[3**]

[1]Department of Electronics and Electrical Engineering, Lorestan University, Khoramabad, I. R. of Iran
[2]Centre of Excellence for Power System Automation and Operation, Department of Electrical Engineering, Iran University of Science and Technology, Narmak, Tehran 16844, I. R. of Iran
[3]Department of Electronics and Electrical Engineering, Shiraz University of Technology, Shiraz, I. R. of Iran
Email: gitizadeh@sutech.ac.ir

Abstract– Modal interaction noticeably affects the dynamic behavior of a stressed power system with heavy loading. In this paper, Modal Series (MS) as a method to analyze modal interactions is extended for a power system installed with a static synchronous series compensator (SSSC) stabilizer. The ϕ- based and *m*-based stabilizers as two stabilizers in different control channels are presented for a SSSC. The parameters of the stabilizers are calculated by a quadratic mathematical programming method. In this procedure, the gain and the phase of a stabilizer are calculated simultaneously. A particular measure of stabilizer gain is considered as an objective function. The effects of SSSC based stabilizers on damping inter-area oscillations for a small disturbance are studied and compared. Modal interactions between an inter-area mode and control modes related to SSSC stabilizers are studied by a proposed index based on MS method in a 4-machine stressed power system. Oscillatory instability caused by modal interactions is investigated and compared in the system for both SSSC stabilizers.

Keywords– Inter-area oscillations, static synchronous series compensator (SSSC), damping stabilizer, nonlinear modal interactions, stressed power systems

1. INTRODUCTION

In steady state, SSSC is one of the series flexible AC transmission systems (FACTS) that injects a balanced three phase voltage to a transmission line and quadrature with the line current [1]. Therefore, in this situation it can only exchange the reactive power with the network. Also, in dynamic state it can exchange active power with the network. SSSC when equipped with a suitable stabilizer can damp power oscillations [2]. There are two channels to control the magnitude and phase of the injected voltage. A stabilizer can be applied to both channels to damp mechanical oscillations. For convenience, the stabilizer in the phase control channel is called ϕ- based and in the magnitude control channel is called *m*-based stabilizer. In studying small disturbance stability, the ϕ- based stabilizer is more effective in damping inter-area oscillations compared to the *m*-based stabilizer [3]. When a stressed power system is faced with partly severe disturbance, nonlinear modal interactions are increased and the dynamic behavior of the system will be complex [4]. In these conditions, modal interactions may deteriorate damping of an inter-area mode and consequently the system may be unstable [5-7]. In past decades, to analyze the modal interactions in stressed power systems, the normal form (NF) method was one of the proposed methods [8-11]. Although the applications of this method are reported in many areas and regarded as a useful and

*Received by the editors January 29, 2012; Accepted December 15, 2012.
**Corresponding author

effective tool, there are a few drawbacks to this method. This method needs to do nonlinear transformations as well as solving nonlinear algebraic equations. Also, in this method resonance and quasi-resonance conditions must not be satisfied. Modal series is another method that has been proposed recently to analyze the nonlinear behavior of stressed power systems [12, 13]. The modal series method retains most of the advantages of the NF method, without having the mentioned drawbacks.

Modal interactions in a power system installed with FACTS based stabilizers has not been satisfactorily addressed. Among FACTS devices, the Static VAR Compensator (SVC) and Unified Power Flow Controller (UPFC) have been studied in this field of research [14-18].

In this paper, a lead-lag stabilizer is considered for a SSSC. The gain and phase of the stabilizer are simultaneously calculated by a quadratic mathematical programming method. The modal series method is extended to a power system with a SSSC stabilizer. The approximate responses of a 4-machine power system by linear and modal series methods are compared by a proposed index. Modal interactions between inter-area mode and control modes related to SSSC stabilizers are investigated by a proposed index. Effects of modal interactions on stability of the system with SSSC stabilizer in both control channels are investigated and compared.

2. POWER SYSTEM MODEL

a) Generator

In this study, each generator is represented by a fourth-order d-q axis model. Therefore, nonlinear dynamic equations for i^{th} generator with known variables are as follows [19]:

$$\dot{\delta}_i = \omega_i - \omega_s \tag{1}$$

$$M_i \dot{\omega}_i = P_{mi} - (I_{di} E'_{di} + I_{qi} E'_{qi}) + (X'_{qi} - X'_{di}) I_{di} I_{qi} - D(\frac{\omega_i}{\omega_s} - 1) \tag{2}$$

$$T'_{d0i} \dot{E}'_{qi} = E_{FDi} - E'_{qi} - (X_{di} - X'_{di}) I_{di} \tag{3}$$

$$T'_{q0i} \dot{E}'_{di} = +E'_{di} - (X_{qi} - X'_{qi}) I_{qi} \tag{4}$$

b) Exciter

In this paper, the IEEE type-AC-4A excitation system is considered, the block diagram is shown in Fig. 1. The role of used parameters for the system is discussed in [20].

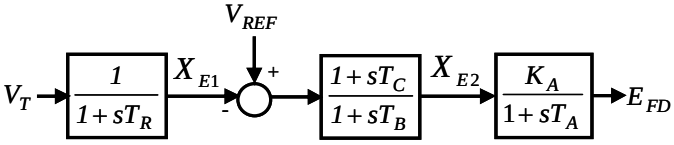

Fig. 1. Excitation system

c) SSSC modeling

It is assumed that, in an n-machine power system, a SSSC is installed on the transmission line between nodes 1 and 2 as shown in Fig. 2.

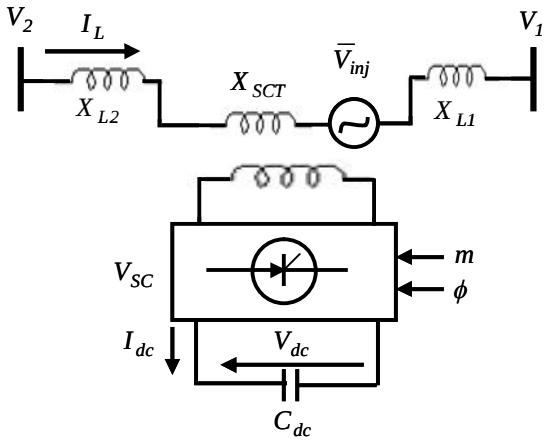

Fig. 2. SSSC structure

The SSSC consists of a series coupling transformer (SCT) with the leakage reactance $X_{SCT,}$ a three-phase GTO based voltage source converter (VSC) and a DC capacitor. The SSSC can be described as [21]:

$$V_{inj} = mkV_{dc}(\cos\phi + j\sin\phi) \tag{5}$$

$$I_L = I_D + jI_Q = |I_L|\angle\psi \tag{6}$$

$$\frac{dV_{dc}}{dt} = \frac{mk}{C_{dc}}(I_D\cos\phi + I_Q\sin\phi) \tag{7}$$

where V_{inj} is the injected ac voltage by the SSSC; m and ϕ are the modulation ratio and phase defined by pulse width modulation (PWM), respectively; depending on the converter structure k is the ratio between the ac and dc voltage; V_{dc} is the dc voltage; C_{dc} is the capacitance of the dc capacitor, and I_D and I_Q are D- and Q components of the line current I_L, respectively.

3. SSSC-BASED STABILIZERS

a) Phase-based stabilizer

Assuming a lossless SSSC, the ac voltage is kept in quadrature with the line current so that the SSSC only exchanges reactive power with the transmission line. By adjusting the magnitude of the injected voltage, the reactive power exchange can be controlled. When the SSSC voltage lags the line current by 90º, it emulates a series capacitor, when the voltage leads the line current by 90º it can also emulate a series inductor. Thus, a SSSC can be considered as a series reactive compensator, where the degree of compensation can be varied by controlling the magnitude of the injected voltage. In this paper, the SSSC is considered in capacitive mode. To keep the injected voltage in quadrature with the line current, a PI controller, as shown in Fig. 3, has been used. Here, ϕ_{ref} is the phase of the injected voltage in steady-state and its value is considered as $\phi_{ref} = -90^o + \psi_{ss}$, where ψ_{ss} is the angle of the line current in steady-state; *Tsssc* is the time constant of the converter, K_P and K_I are the proportional and integral gains of the PI controller, respectively. In the PI controller, a lead-lag stabilizer for damping the inter-area oscillations is included. In this case, the stabilizer is called the phase-based stabilizer and for convenience in this paper, it is called ϕ-based stabilizer. In this stabilizer, T_W is the washout time constant; T is the stabilizer time constant, and x_2, x_1 and x_0 are parameters to be determined. The feedback signal for the stabilizer is selected among local signals as the line-current, the line-real power, and the line-reactive power.

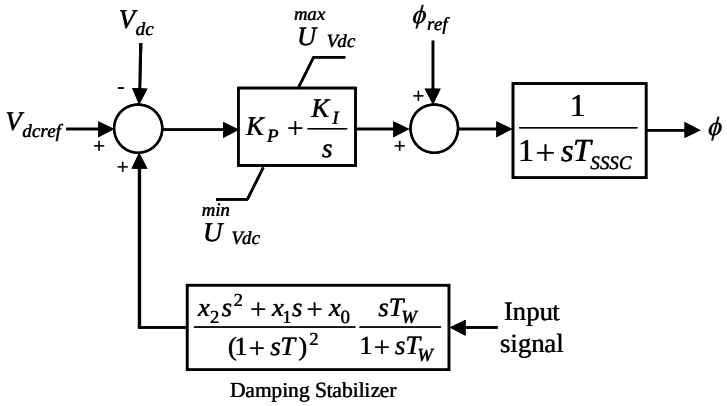

Fig. 3. SSSC phase controller with a damping stabilizer

b) Magnitude-based stabilizer

In order to control the magnitude of the injected voltage, the modulation ratio *m* can be controlled. Fig. 4 shows the block diagram of the controller in this case, where X_{ref} is the value of produced series reactance by SSSC in capacitive mode, in steady state condition. A stabilizer for damping of inter-area oscillations is included in the magnitude controller. This stabilizer is called *m*-based stabilizer**.**

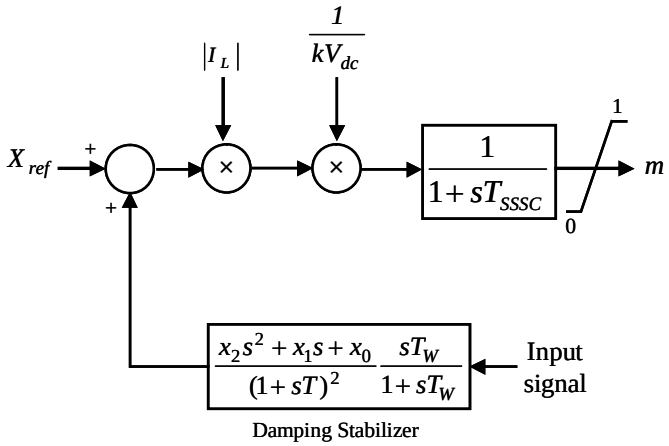

Fig. 4. SSSC magnitude controller with a damping stabilizer

4. QUADRATIC MATHEMATICAL PROGRAMMING TO DESIGN THE STABILIZER

The design method used in this paper is an incremental method including two steps. In the first step, the closed-loop system is considered as in Fig. 5, where *G(s)* and $\overline{F}(s)$ are the power system transfer matrix and the stabilizer transfer matrix, respectively. In the second step, the stabilizer transfer matrix is changed by *ΔF*. In this case, the closed-loop system changes as shown in Fig. 6, where $\overline{G}(s)$ is the transfer matrix of the inner loop between *G(s)* and $\overline{F}(s)$.

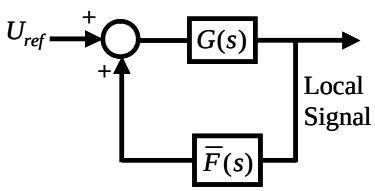

Fig. 5. Closed loop system in the first step

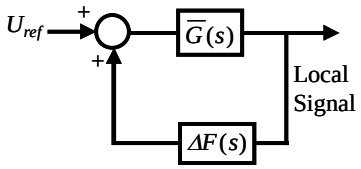

Fig. 6. Closed loop system in the second step

The details of the method for calculation ΔF are presented in [3]. This method is summarized as follows. Assuming variations of ΔF are sufficiently small, the variation of the eigenvalue λ_i can be approximated as:

$$\Delta\lambda_i = \rho_i \, \Delta f(\lambda_i) \quad (i=1, 2, ..., n) \tag{8}$$

where n is the number of critical eigenvalues and ρ_i is the residue associated to the i^{th} eigenvalue λ_i of $\overline{G}(s)$.

It is assumed that the stabilizer has a lead-lag structure as follows:

$$f(s) = \frac{x_2 s^2 + x_1 s + x_0}{(1+sT)^2} \frac{sT_w}{1+sT_w} \tag{9}$$

By substituting $s = \lambda_i$ and $x_m = \Delta x_m$ (m=1, 2, 3) in (9), the real and imaginary part variations of $\Delta f(\lambda_i)$ can be obtained as a linear function of Δx_0, Δx_1 and Δx_2. Then, by substituting the real and imaginary parts of $\Delta f(\lambda_i)$ in (8), the real and imaginary parts of $\Delta\lambda_i$ can be written as a linear function of Δx_0, Δx_1 and Δx_2. Considering $\Delta\sigma_i$ and $\Delta\omega_i$ as the desired values of the real and imaginary parts of the critical eigenvalue λ_i, respectively, the following constraints can be obtained to shift the critical eigenvalues to the desired areas in the complex plane [3].

$$\alpha_{2i}\Delta x_2 + \alpha_{1i}\Delta x_1 + \alpha_{0i}\Delta x_0 \le -\left|\Delta\sigma_i\right| \tag{10}$$

$$-\left|\Delta\omega_i\right| \le \beta_{2i}\Delta x_2 + \beta_{1i}\Delta x_1 + \beta_{0i}\Delta x_0 \le \left|\Delta\omega_i\right| \tag{11}$$

where α_{0i}, α_{1i}, α_{2i}, β_{0i}, β_{1i}, and β_{2i} are specified values. On the other hand, if the angle of residue ρ_i is positive, the stabilizer must have a phase-lead characteristic; otherwise, it must have a phase-lag characteristic. For a phase–lead structure, it is assumed that zeros of the stabilizer are almost one decade closer to the imaginary axis than that of its poles and for the phase-lag structure the zeros are almost one decade farther to the imaginary axis. Considering $x_m = \bar{x}_m + \Delta x_m$ (m=1, 2, 3), the constraints on zeros can be written for a lead-phase stabilizer as in (12) to (14) and for a phase-lag stabilizer as in (15) to (17) [3].

$$-\Delta x_2 + T\Delta x_1 - T^2\Delta x_0 \le \bar{x}_2 - T\bar{x}_1 + T^2\bar{x}_0 \tag{12}$$

$$-\Delta x_2 + 10T\Delta x_1 - 100T^2\Delta x_0 \le \bar{x}_2 - 10T\bar{x}_1 + 100T^2\bar{x}_0 \tag{13}$$

$$18\Delta x_2 - 99T\Delta x_1 + 180T^2\Delta x_0 \le -18\bar{x}_2 + 99T\bar{x}_1 - 180T^2\bar{x}_0 \tag{14}$$

$$-\Delta x_2 + T\Delta x_1 - T^2\Delta x_0 \le \bar{x}_2 - T\bar{x}_1 + T^2\bar{x}_0 \tag{15}$$

$$-100\Delta x_2 + 10T\Delta x_1 - T^2\Delta x_0 \le +100\bar{x}_2 - 10T\bar{x}_1 + T^2\bar{x}_0 \tag{16}$$

$$180\Delta x_2 - 99T\Delta x_1 + 18T^2\Delta x_0 \le -180\bar{x}_2 + 99T\bar{x}_1 - 18T^2\bar{x}_0 \tag{17}$$

where $\bar{x}_0$, $\bar{x}_1$ and $\bar{x}_2$ are known values.
The following function, as the gain of the stabilizer at the frequency $\bar{\omega}_i$, i=1, 2, . . . m, is considered as the objective function [3].

$$J = \min \sum_{i=1}^{m} \left| f\left(j\bar{\omega}_i\right) \right|^2 \tag{18}$$

where $\bar{\omega}_1$, $\bar{\omega}_2$..., $\bar{\omega}_m$ are a set of frequencies in the region where the critical eigenvalue must be shifted.

By substituting (9) in (18) and considering $s = j\bar{\omega}_i$, we can easily rewrite the objective function as

$$J = \min \frac{1}{2}\Delta X^T H \Delta X + f^T \Delta X \tag{19}$$

where the matrix H and vector f are known and $\Delta X = [\Delta x_2 \;\; \Delta x_1 \;\; \Delta x_0]^T$ is the unknown vector to be tuned. The objective function (19) along with constraints (10)-(11) and (12)-(14) or (15)-(17) forms a quadratic mathematical programming problem. To solve this problem, the function of *quadprog* embedded in Matab Optimization Toolbox is applied here.

5. ZERO INPUT RESPONSE USING LINEAR AND MODAL SERIES METHODS

The dynamic behavior of a power system can be represented by a set of nonlinear equations as follows:

$$\dot{X} = F(X) \tag{20}$$

where $X \in R^N$ is the state vector and $F : R^N \to R^N$ is a smooth vector field.
Let X_{SEP} be a stable equilibrium point (SEP) of the system. By expanding the Taylor series around X_{SEP}, the equation (20) can be written as:

$$\dot{X}_i = A_i X + \frac{1}{2} X^T H^i X + \ldots \tag{21}$$

where A_i is i^{th} row in Jacobeans matrix $A = \left[\frac{\partial F}{\partial X}\right]_{X_{SEP}}$ and $H^i = \left[\frac{\partial^2 F_i}{\partial x_k \partial x_l}\right]_{X_{SEP}}$ is the i^{th} $N \times N$ sized hessian matrix.
Let the right and left eigenvectors of matrix A be considered as U and V, respectively. Assuming the eigenvalues of matrix A are distinct, using the transformation $X=UY$, equation (21) can be written in the Jordan form as:

$$\dot{y}_j = \lambda_j y_j + \sum_{k=1}^{N}\sum_{l=1}^{N} C_{kl}^j y_k y_l + \cdots \tag{22}$$

where $C^j = \frac{1}{2}\sum_{p=1}^{N} V_{jp}^T \left[U^T H^p U\right] = \left[C_{kl}^j\right]$

a) Linear modal method

In the linear modal method, only the first term in (21) is considered and higher order terms are omitted. In this case, the linear solution for j^{th} Jordan variable will be as:

$$y_j(t) = y_{jo} e^{\lambda_j t} \tag{23}$$

where y_{j0} is j^{th} element in vector of $Y_0 = U^{-1} X_0$ and X_0 is the initial condition vector in physical state – space.

Using transformation $Y = U^{-1} X$, the approximate solution for i^{th} state variable in the original space would be as:

$$x_i(t) = \sum_{j=1}^{N} u_{ij} y_j(t) = \sum_{j=1}^{N} u_{ij} y_{j0} e^{\lambda_j t} \tag{24}$$

where u_{ij} is the i, j element of the right eigenvector matrix U.

b) Modal series method

In this method, beside linear terms, second order terms are also considered, but third and higher order terms are ignored.

In this case, second order closed form approximate solution of (22) for j^{th} state variable in the Jordan form will be as[12, 13]:

$$\begin{aligned} y_j(t) \approx & \left(y_{j0} - \left\{ \sum_{k=1}^{N} \sum_{l=1}^{N} h2_{kl}^{j} y_{ko} y_{lo} \right\}_{(k,l,j) \notin R_2'} \right) e^{\lambda_j t} \\ & + \left\{ \sum_{k=1}^{N} \sum_{l=1}^{N} h2_{kl}^{j} y_{ko} y_{lo} e^{(\lambda_k + \lambda_l)t} \right\}_{(k,l,j) \notin R_2'} \\ & + \left\{ \left[\sum_{k=1}^{N} \sum_{l=1}^{N} C_{kl}^{j} y_{ko} y_{lo} \right] t e^{\lambda_j t} \right\}_{(k,l,j) \in R_2'} \end{aligned} \tag{25}$$

where $h2_{kl}^{j} = C_{kl}^{j} / (\lambda_k + \lambda_l - \lambda_j)$ and R_2' is all three triples(k,l,j) which satisfy the second order resonance conditions $\lambda_k + \lambda_l = \lambda_j$. The second order approximate solution in the physical space can be represented as:

$$x_i(t) = \sum_{j=1}^{N} u_{ij} y_j(t) = \sum_{j=1}^{N} \left(L_j^i + M_j^i t \right) e^{\lambda_j t} + \sum_{k=1}^{N} \sum_{l=1}^{N} K_{kl}^i e^{(\lambda_k + \lambda_l)t} \tag{26}$$

where :

$$L_j^i = uij \left(y_{j0} - \left\{ \sum_{k=1}^{N} \sum_{l=1}^{N} h2_{kl}^{j} y_{k0} y_{l0} \right\}_{(k,l,j) \notin R_2'} \right)$$

$$K_{kl}^i = \left[y_{k0} y_{l0} \sum_{j=1}^{N} u_{ij} h2_{kl}^{j} \right]_{(k,l,j) \notin R_2'}$$

$$M_j^i = \left[\sum_{k=1}^{N} \sum_{l=1}^{N} u_{ij} C_{kl}^{j} y_{k0} y_{l0} \right]_{(k,l,j) \in R'_2}$$

Comparing the coefficients of individual and combination modes in (25) for j^{th} Jordan variable leads to the definition of the nonlinear interaction index as follows [22].

$$II(j)=\left|\frac{\max\limits_{k,l} h2_{kl}^{j} y_{k0} y_{l0}}{y_{j0}-\max\limits_{k,l} h2_{kl}^{j} y_{k0} y_{l0}}\right| \tag{27}$$

where $\max\limits_{k,l} h2_{kl}^{j} y_{k0} y_{l0}$ is the complex form when $\max\limits_{k,l}\left|h2_{kl}^{j} y_{k0} y_{l0}\right|$ occurs.

6. SIMULATION RESULTS

The test system here is a 2-area 4-machine power system. A single line diagram of the system is shown in Fig. 7 [23]. To control inter-area oscillations, a SSSC is installed in the tie-line between nodes 5 and 6. Data of this system and specific parameters used for the SSSC are given in the Appendix. The loads are modeled as constant impedances. No PSS is installed in the system. To increase transferred power, the load in area 2 has been increased and the load in area 1 has then been modified to achieve a given tie-line transferred power.

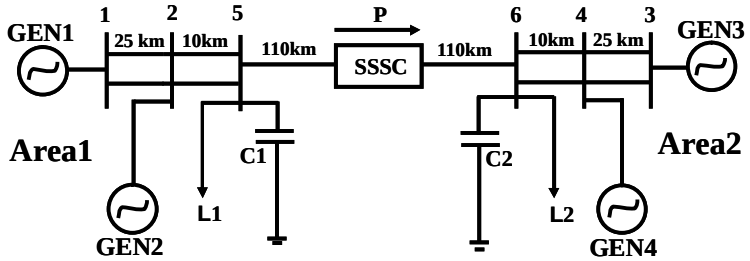

Fig. 7. One line-diagram of the test system

Table 1. Studied operating conditions

Loading conditions	Load of Area 1(MW)	Load of Area 2(MW)	Transmitted power(MW)
Low stress	1000	1300	310
High stress	890	1410	410

Summary of studied operating conditions are shown in Table 1. The oscillation modes in the open loop system for low and high stress loading conditions are shown in Table 2. This table shows that damping of inter-area mode is low, particularly in high stress conditions. To increase damping of this mode to a desirable value, the parameters of SSSC ϕ-based and *m*-based stabilizers are calculated by a quadratic mathematical programming method. The variation of line current magnitude is considered as the best input signal for both SSSC stabilizers [3]. As the desired damping ratio for inter-area mode, typically two values of ζ=7% for high stress loading conditions and ζ=10% for low stress loading conditions have been considered. The time constant of the stabilizers is considered to be T=0.4 s. Parameters of stabilizers to achieve desired damping ratios of inter-area mode are shown in Table 3. Loop gains of the stabilizers ($|f(j\omega)|$) in a frequency close to frequency of inter-area mode are shown in the last column of the table. Typically, this frequency is considered as ω=1.7 rad/s. This value is average of inter-area mode frequency for different SSSC stabilizer and different operation conditions. Table 3 shows that for the same desired damping ratio, the loop gains of the SSSC ϕ-based stabilizer is less than the SSSC *m*-based stabilizer. That is, to achieve the same desired damping ratio for inter-area mode, control cost in the SSSC ϕ-based stabilizer is lower compared with the SSSC *m*-based stabilizer. In other words, the SSSC ϕ-based stabilizer is more effective for damping inter-area oscillations. Oscillation modes in closed loop systems for SSSC ϕ and *m*-based stabilizer are shown in Tables 4 to 6. These tables show that damping ratio of inter-area mode has been improved to the desired value. In addition, it can be seen that the other modes have not been degraded significantly. Also, these tables show that the SSSC stabilizers create new control oscillation modes.

Table 2. Oscillation modes in open loop system

Mode #	P=310 MW		P=410 MW		Dominant states
	Eigenvalue	Damping (%)	Eigenvalue	Damping (%)	
1,2	-1.225±j7.728	15.66	-1.244±j7.748	15.85	Local, Area 1(δ_1, δ_2)
3,4	-1.577±j7.451	20.71	-1.554±j7.549	20.16	Local, Area 1(δ_3, δ_4)
5,6	-0.088±j1.787	4.92	-0.028±j1.647	1.70	Inter-area(δ_1, δ_2, δ_3, δ_4)
7,8	-1.151±j0.846	79.97	-1.320±j0.832	84.60	$\omega_1, E'_{q2}, X_{E12}, X_{E22}$
9,10	-0.557±j 0.832	55.63	-0.585±j 0.826	57.79	$E'_{q3}, E'_{q4}, X_{E14}, X_{E24}$
11,12	-0.253±j0.383	55.12	-0.257±j0.393	54.84	Control (Exciter 1)
13, 14	-0.269±j0.358	60.07	-0.284±j0.361	61.79	Control(Exciter 3 and 4)

Table 3. Parameters of SSSC damping stabilizers

P(MW)	ζ(%)	SSSC stabilize	x_2	x_1	x_0	$\lvert f(j\omega)\rvert$
410	7	*m*-based	0.08602	0.04301	0.00538	0.1737
		ϕ-based	0.00178	0.01169	0.04915	0.0330
	10	*m*-based	0.14440	0.07220	0.00902	0.2915
		ϕ-based	0.00275	0.03395	0.06764	0.0568
310	10	*m*-based	0.45702	1.22090	0.47085	1.5337
		ϕ-based	0.00137	0.00901	0.03837	0.0258

Table 4. Oscillation modes in closed loop system for ζ=10% and P=310 MW

Mode #	SSSC ϕ-based stabilizer		SSSC *m*-based stabilizer		Dominant states
	Eigenvalue	Damping (%)	Eigenvalue	Damping (%)	
1, 2	-1.225±j7.729	15.65	-1.255±j7.660	16.17	Local, Area 1(δ_1, δ_2)
3, 4	-1.577±j7.451	20.71	-1.555±j7.398	20.57	Local, Area 1(δ_3, δ_4)
5, 6	-0.180±j1.789	10.01	-0.181±j1.777	10.13	Inter-area(δ_1, δ_2, δ_3, δ_4)
7, 8	-1.180±j0.891	79.80	-1.199±j1.147	72.26	$\omega_1, E'_{q2}, X_{E12}, X_{E22}$
9, 10	-0.553±j0.857	54.22	-0.548±j0.817	55.70	$E'_{q3}, E'_{q4}, X_{E14}, X_{E24}$
11, 12	-0.253±j0.383	55.18	-0.251±j0.383	54.81	Control (Exciter 1)
13, 14	-0.268±j0.358	59.93	-0.269±j0.358	57.27	Control(Exciter 3 and 4)
15, 16	-0.946±j0.879	73.26	-0.721±j0.611	76.29	Control(SSSC stabilizer)

Table 5. Oscillation modes in closed loop system for ζ=7% and P=410 MW

Mode #	SSSC ϕ-based stabilizer		SSSC *m*-based stabilizer		Dominant states
	Eigenvalue	Damping (%)	Eigenvalue	Damping (%)	
1,2	-1.244±j7.749	15.85	-1.250±j7.751	15.91	Local, Area 1(δ_1, δ_2)
3,4	-1.554±j7.549	20.16	-1.557±j7.548	20.20	Local, Area 1(δ_3, δ_4)
5,6	-0.123±j1.748	7.02	-0.119±j1.692	7.02	Inter-area(δ_1, δ_2, δ_3, δ_4)
7, 8	-1.402±j0.927	83.42	-1.277±j0.739	86.64	$\omega_1, E'_{q2}, X_{E12}, X_{E22}$
9, 10	-0.582±j0.854	56.29	-0.584±j0.826	57.73	$E'_{q3}, E'_{q4}, X_{E14}, X_{E24}$
11, 12	-0.257±j0.393	54.75	-0.257±j0.393	54.82	Control (Exciter 1)
13, 14	-0.283±j0.361	61.68	-0.284±j0.361	61.80	Control(Exciter 3 and 4)
15, 16	-0.552±j0.506	71.80	-0.623±j0.318	89.07	Control(SSSC stabilizer)

For verification of the designed stabilizers a three-phase fault is applied to the test system at bus 6. The clearing time of fault, t_{cr}, is set as t_{cl}=20 ms. The fault is cleared without line switching. Because the generators 1 and 3 have the most contribution in the inter-area mode, typically, swing angle of generator 1 with respect to generator 3 for different SSSC-based stabilizers at high stress operation conditions is shown in Fig. 8. This figure shows that SSSC stabilizers can effectively damp inter-area oscillations.

Table 6. Oscillation modes in closed loop system for ζ=10% and P=410 MW

Mode #	SSSC ϕ-based stabilizer		SSSC *m*-based stabilizer		Dominant states
	Eigenvalue	Damping (%)	Eigenvalue	Damping (%)	
1, 2	-1.244±j7.749	15.85	-1.254±j7.751	15.97	Local, Area 1(δ_1, δ_2)
3, 4	-1.554±j7.549	20.16	-1.559±j7.546	20.24	Local, Area 1(δ_3, δ_4)
5, 6	-0.172±j1.675	10.21	-0.168±j1.644	10.19	Inter-area(δ_1, δ_2, δ_3, δ_4)
7, 8	-1.453±j0.841	86.54	-1.238±j0.704	86.93	$\omega_1, E'_{q2}, X_{E12}, X_{E22}$
9, 10	-0.593±j0.862	56.70	-0.584±j0.827	57.68	$E'_{q3}, E'_{q4}, X_{E14}, X_{E24}$
11, 12	-0.257±j0.393	54.75	-0.257±j0.393	54.82	Control (Exciter 1)
13, 14	-0.283±j0.361	61.68	-0.284±j0.361	61.80	Control(Exciter 3 and 4)
15, 16	-0.568±j0.694	63.34	-0.478±j0.523	67.46	Control(SSSC stabilizer)

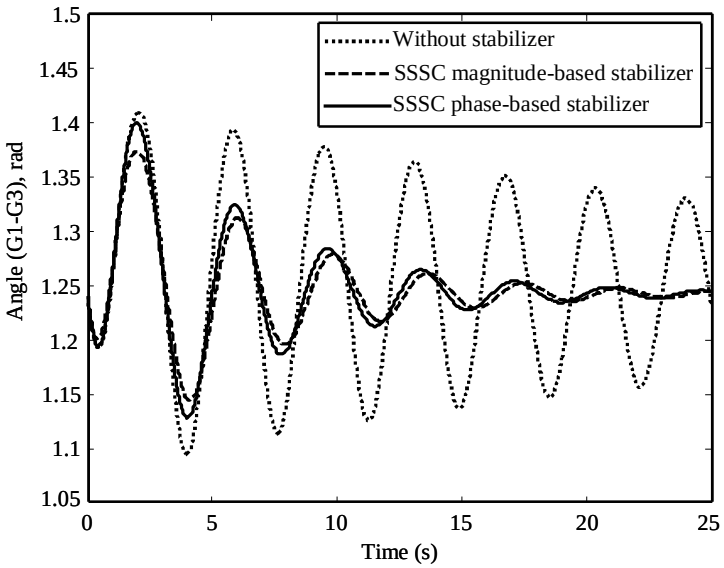

Fig. 8. Response of system without and with SSSC stabilizer for ζ=10%, P=410 MW and t_{cl}=20 ms

The response of the closed loop system for t_{cl}=15 ms and 40 ms for SSSC ϕ-based and *m*-based stabilizers are shown in Figs. 9 to 12. In these figures, nonlinear simulation as a full solution and approximate solutions are shown. These figures show that when fault duration is small, the full nonlinear solution and approximate solutions are very close to each other. But, when fault duration is increased, the difference between full solution and approximate solutions is noticeable. In this case, nonlinear modal interactions are increased. Also, it can be seen that approximate solution by modal series method is always close to full solution in comparison with linear modal solution. Therefore, in a stressed power system faced with a severe fault, linear modal analysis cannot evaluate dynamic behavior of the system well.

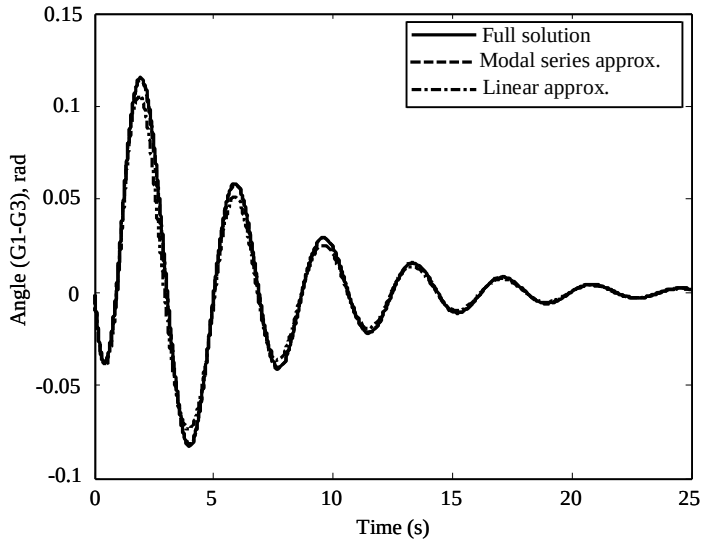

Fig. 9. Response of system with ϕ-based stabilizer for ζ=10%, P=410 MW and t_{cr}=15 ms

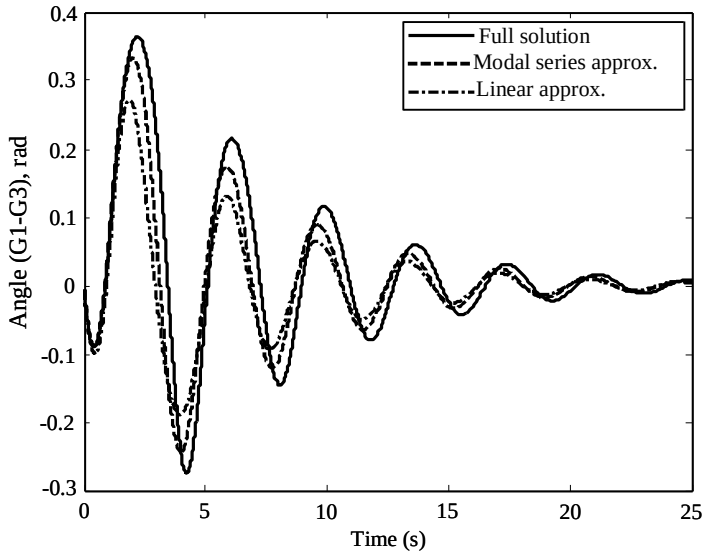

Fig. 10. Response of system with ϕ-based stabilizer for ζ=10%, P=410 MW and t_{cr}=40 ms

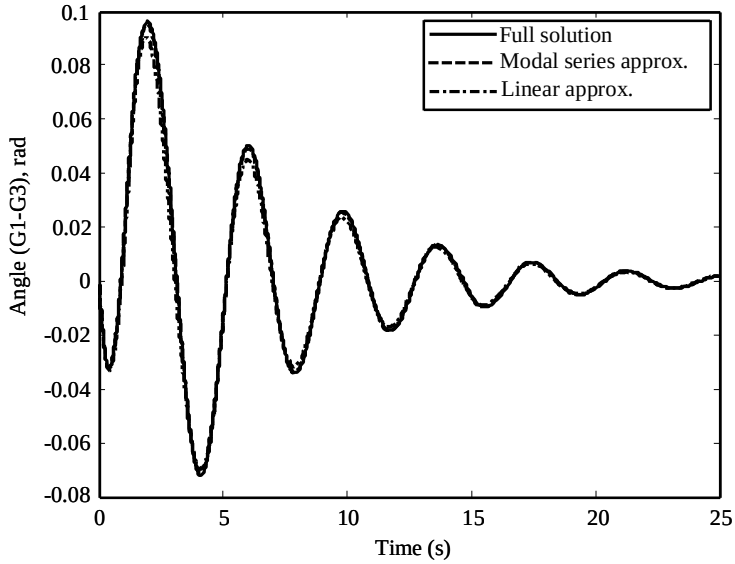

Fig. 11. Response of system with *m*-based stabilizer for ζ=10%, P=410 MW and t_{cr}=15 ms

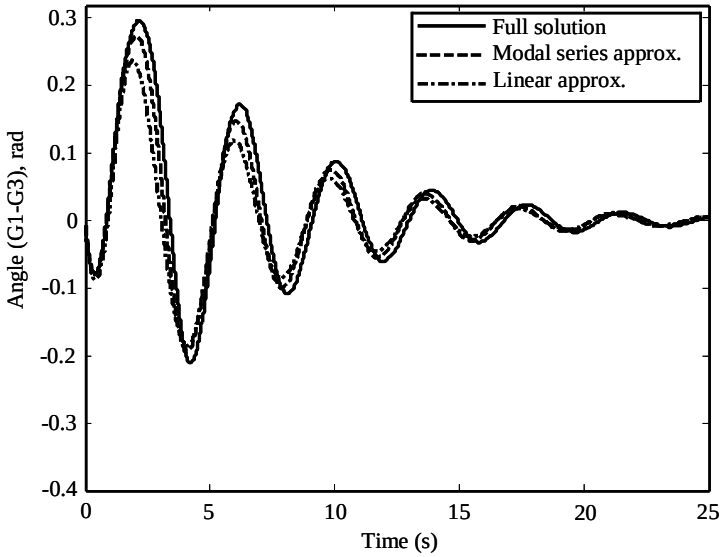

Fig. 12. Response of system with *m*-based stabilizer for ζ=10%, P=410 Mw and t_{cr}=40 ms

To evaluate the precision of the approximate solutions, an error index is used as follows [24].

$$Er(i) = \frac{1}{T}\int_0^T \left| x_i(t) - \tilde{x}_i(t) \right| dt \tag{28}$$

where, T is the simulation time, $x_i(t)$ and $\tilde{x}_i(t)$ are full and approximate response for i^{th} state variable, respectively.

According to (28), the error index for different values of fault duration for closed loop system in high stress loading conditions for different SSSC stabilizers is shown in Fig. 13. This figure shows that when fault duration is increased the error index for the system with *m*-based stabilizer is lower in comparison with ϕ-based stabilizer. In other words, the nonlinear effects are higher in the system with ϕ-based stabilizer. Also, this figure shows that for different values of fault duration, the error index for approximate response obtained by the modal series is lower than the approximate response obtained by the linear method.

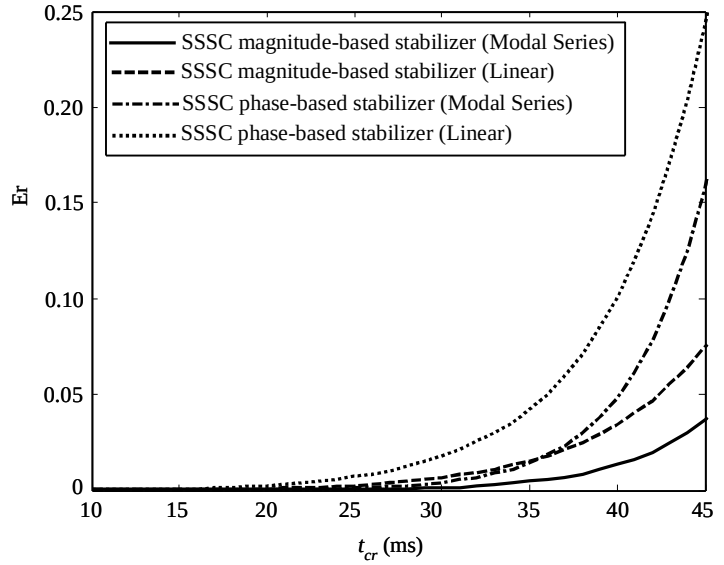

Fig. 13. The value of error index for different values of fault durations in the closed loop system for ζ=10% and P=410 MW

According to (27), in some cases, the values of nonlinear modal interaction index for inter-area mode at fault duration of 35 ms are calculated and shown in Tables 7 to 10. According to these tables, the following results can be concluded:

I. According to Table 7, modal interactions between inter-area mode and control modes related to exciters are not severe in the open loop system.

II. Tables 8 to 10 show that, in the closed loop system, modal interactions between inter-area mode and control modes related to SSSC stabilizers are higher than that of exciter control modes.

III. Comparing Tables 8 and 10 shows that by increasing stress on the system, modal interactions between inter-area mode and SSSC stabilizer control modes are increased.

IV. It can be seen from Tables 8 to 10 that modal interactions between inter-area mode and control mode related to SSSC ϕ-based stabilizer are higher than the *m*-based stabilizer.

V. From Tables 8 and 10, it can be concluded that by increasing desired damping ratio, for inter-area mode in a certain value of transferred power, the modal interactions between inter-area mode and SSSC stabilizer control modes are increased.

Table 7. Nonlinear modal interaction index for inter-area mode in the open loop system for P=410 MW

Mode *j*	Mode *k*	Mode *l*	*II*(*j*)
5	5	11	0.62
	7	11	0.42
	9	13	0.37
	5	5	0.11

Table 8. Nonlinear modal interaction index for inter-area mode in the closed loop system for ζ=10% and P=310 MW

SSSC stabilizer	Mode *j*	Mode *k*	Mode *l*	*II*(*j*)
ϕ-based	5	15	15	1.89
		5	15	0.93
		7	11	0.28
		9	13	0.19
m-based	5	15	15	0.95
		5	15	0.56
		9	11	0.21
		7	13	0.20

Table 9. Nonlinear modal interaction index for inter-area mode in the closed loop system for ζ=7% and P=410 MW

SSSC stabilizer	Mode *j*	Mode *k*	Mode *l*	*II*(*j*)
ϕ-based	5	15	15	3.18
		5	15	1.72
		7	11	0.72
		9	13	0.59
m-based	5	15	15	1.84
		5	15	0.87
		9	11	0.61
		7	13	0.53

Table 10. Nonlinear modal interaction index for inter-area mode in the closed loop system for ζ=10% and P=410 MW

SSSC stabilizer	Mode *j*	Mode *k*	Mode *l*	*II*(*j*)
ϕ-based	5	15	15	4.11
		5	15	2.17
		7	11	0.69
		9	13	0.56
m-based	5	15	15	2.32
		5	15	1.18
		9	11	0.59
		7	13	0.57

For more stress on the system, loads L_1 and L_2 are set in the values 1430 and 870 MW, respectively. In this case, transferred power between two areas is about P=430 MW. The mechanical and control oscillation modes in the open loop system are shown in Table 11. This table shows that inter-area mode is unstable for this condition. Mechanical and control modes in the closed loop system, with parameters of Table 3 related to P=410 MW and ζ=10%, are presented in Table 12. This table shows that damping ratio of inter-area mode in the closed loop system has been reduced by increasing transmitted power. Also, it can be seen from this table that the damping of inter-area mode with the ϕ-based stabilizer is somewhat higher than the *m*-base stabilizer. Swing angle of generator 1 with respect to generator 3 for the ϕ-based and *m*-based stabilizer at different values of fault duration are shown in Figs. 14 and 15, respectively. Figure 14 shows that when fault clearing time is 10 ms (small disturbance) the system is stable. This condition is coincident with eigenvalue results. By increasing fault duration to t_{cr}=25.3 ms, damping of oscillations would be approximately zero and the oscillations are repeated periodically without decaying or diverging. Lastly, in fault duration of 26.5 ms, the system is faced with oscillatory instability and loses its synchronism after about 20 seconds.

Table 11. Oscillation modes in the open loop system for P=430 MW

Mode #	Eigenvalue	Damping (%)	Dominant states
1,2	-1.247±j7.760	15.87	Local, Area 1(δ_1, δ_2)
3,4	-1.539±j7.585	19.88	Local, Area 1(δ_3, δ_4)
5,6	0.024±j1.476	-1.63	Inter-area(δ_1, δ_2, δ_3, δ_4)
7, 8	-1.431±j0.718	89.38	$\omega_1, \omega_3, E'_{q2}, X_{E12}, X_{E22}$
9, 10	-0.584±j0.822	57.92	$E'_{q3}, E'_{q4}, X_{E14}, X_{E24}$
11, 12	-0.257±j0.397	54.34	Control (Exciter 1)
13,14	-0.288±j0.361	62.36	Control(Exciter 3 and 4)

Table 12. Oscillation modes in the closed loop system (with parameters of Table 3 related to P=410 MW and ζ=10%) for P=430 MW

Mode #	SSSC ϕ-based stabilizer		SSSC *m*-based stabilizer		Dominant states
	Eigenvalue	Damping (%)	Eigenvalue	Damping (%)	
1,2	-1.246±j7.760	15.85	-1.256±j7.763	15.97	Local, Area 1(δ_1, δ_2)
3,4	-1.539±j7.585	19.88	-1.543±j7.583	19.94	Local, Area 1(δ_3, δ_4)
5,6	-0.052±j1.432	3.63	-0.043±j1.419	3.03	Inter-area(δ_1, δ_2, δ_3, δ_4)
7, 8	-1.662±j0.684	92.47	-1.224±j0.616	89.33	$\omega_1, \omega_3, E'_{q2}, X_{E12}, X_{E22}$
9, 10	-0.595±j0.859	56.94	-0.580±j0.823	57.61	$E'_{q3}, E'_{q4}, X_{E14}, X_{E24}$
11, 12	-0.256±j0.398	54.10	-0.257±j0.397	54.34	Control (Exciter 1)
13, 14	-0.288±j0.362	62.26	-0.288±j0.361	62.36	Control(Exciter 3 and 4)
15, 16	-0.534±j0.756	57.69	-0.452±j0.501	66.99	Control(SSSC stabilizer)

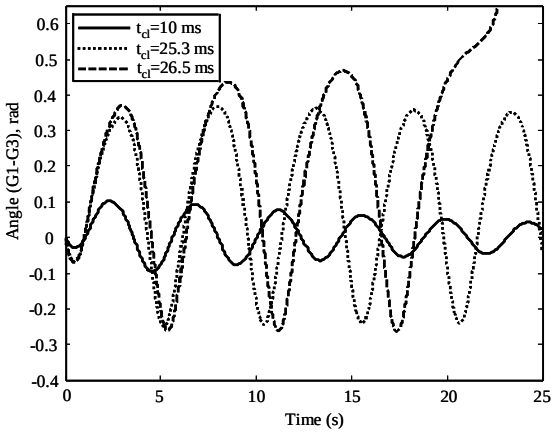

Fig. 14. Response of the system for SSSC ϕ-based stabilizer (with parameters of Table 3 related to P=410 MW and ζ=10%) for P=430 MW at different values of fault duration

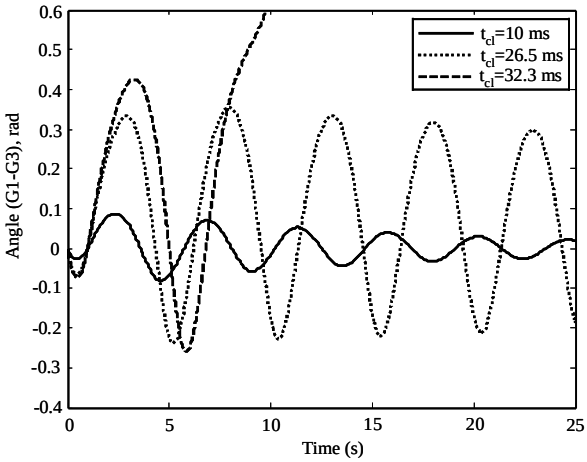

Fig. 15. Response of the system for SSSC *m*-based stabilizer (with parameters of Table 3 related to P=410 MW and ζ=10%) for P=430 MW at different values of fault duration

The fault clearing time for first swing instability for both SSSC stabilizers is shown in Fig. 16. Comparing Figs.14 and 16, it can be seen that fault clearing time for oscillatory instability is about 8 ms less than the clearing time for the first swing instability. Figure 15 shows that the system with SSSC *m*-based stabilizer at t_{cl}=26.5 ms is stable (unlike ϕ-base stabilizer). Also, comparing this figure to Fig. 16 shows that fault clearing time for instability of the system is close to that of for first swing instability.

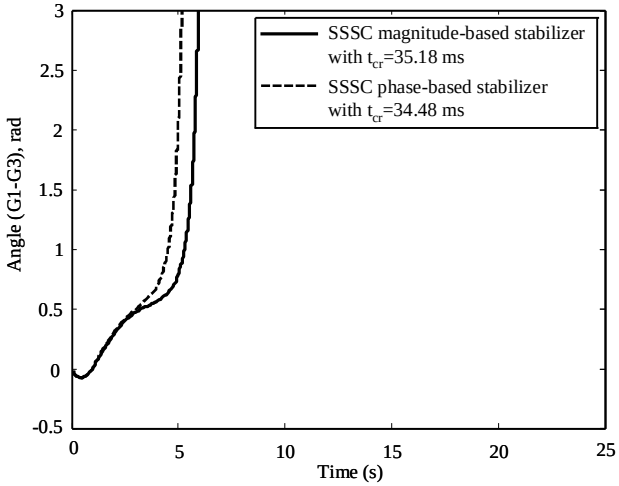

Fig. 16. Response of the system with SSSC based stabilizers (with parameters of Table 3 related to P=410 MW and ζ=10%) for P=430 MW for first swing instability

For P=410 MW, modal interaction index between inter-area mode and SSSC stabilizer control modes for fault duration of 25 ms is shown in Table 13. This table confirms that modal interactions for SSSC ϕ-based stabilizer are severe in comparison with *m*-based stabilizer.

It can be seen from the above results that modal interactions can deteriorate damping of a mechanical mode that causes the system to become unstable. However, the system is recognized as stable due to a small disturbance.

Table 13. Nonlinear modal interaction index for inter-area mode in the closed loop system (with parameters of Table 3 related to P=410 MW and ζ=10%) for P=430 MW

SSSC stabilizer	Mode *j*	Mode *k*	Mode *l*	*II*(*j*)
ϕ-based	5	15	15	5.68
		5	15	3.17
		7	11	0.98
		9	13	0.86
m-based	5	15	15	3.38
		5	15	2.10
		9	11	1.06
		7	13	0.92

7. CONCLUSION

In this paper, modal series method is extended to a multi-machine power system installed with a SSSC-based stabilizer. Phase and magnitude control channels are considered for the SSSC stabilizer. Parameters of the SSSC stabilizer are calculated by a quadratic mathematical programming method. Results show that for small disturbance analysis (eigenvalue analysis), the gain (the control cost) of the stabilizer to improve damping of an inter-area oscillation mode to a desired value with SSSC ϕ-based stabilizer is less than the *m*-based stabilizer. By increasing the fault duration (magnitude of disturbance) in certain operating conditions, modal interactions between inter-area mode and control mode related to SSSC ϕ-based stabilizer are higher than the *m*-based stabilizer. Also, results show that in a certain heavy loading condition, the system with ϕ-based stabilizer is faced with an oscillatory instability whose clearing time is less noticeable than that for the first swing instability. Therefore, to select the optimal control channel for a SSSC stabilizer, in stressed power systems in which modal interactions between an inter-area mode and control modes are high, eigenvalue analysis (small disturbance analysis) alone may not be sufficient and effects of modal interactions must be considered. In other words, a trade-off between linear and nonlinear analysis must be done.

REFERENCES

1. Gyugyi, L., Schauder, C. D. & Sen, K. K. (1997). Static synchronous series compensator: a solid-state approach to the series compensation of transmission lines. *IEEE Trans. Power. Deliv.*, Vol. 12, No. 1, pp. 406-417.
2. Ghaisari, J. & Bakhshai, A. (2006). An advanced robust MIMO SSSC control technique for power oscillation damping improvement. *Iranian Journal of Science and Technology, Transaction B: Engineering*, Vol. 30, No. B6, pp. 667-679.
3. Shakarami, M. R. & Kazemi, A. (2011). Assessment of effect of SSSC stabilizer in different control channels on damping inter-area oscillations, *energy. conver. manag., J.*, Vol. 52, No. 3, pp. 1622-1629.
4. Vittal, V., Bhatia, N. & Fouad, A. A. (1991). Analysis of the inter-area mode phenomenon in power systems following large disturbances. *IEEE Trans. Power Syst.*, Vol. 6, No. 4, pp.1515-1521.
5. Kakimoto, N., Nakanishi, A. & Tomiyama, K. (2004). Instability of Inter-area oscillation mode by auto-parametric resonance. *IEEE Trans. Power syst.*, Vol. 19, No. 4, pp.1961-1970.

6. Amano, H., Kumano, T. & Inoue, T. (2006). Nonlinear stability indexes of power swing oscillation using normal form analysis. *IEEE Trans. Power Syst.*, Vol. 21, No. 2, pp. 825-834.
7. Amano, H. & Inoue, T. (2007). A new PSS parameter design using nonlinear stability analysis. IEEE, Power Engineering Society General Meeting, Tampa, Florida.
8. Lin, C. M., Vittal, V., Kliemann, W. & Foad, A. A. (1996). Investigation of modal interaction and its effects on control performance in stressed power systems using normal forms of vector fields. *IEEE Trans. Power Syst.*, Vol. 11, No. 2, pp. 781-787.
9. Jang, G., Vittal, V. & Klimann, W. (1998). Effect of nonlinear modal interaction on control performance: Use of normal forms technique in control design, Part I: General theory and procedure. *IEEE Trans. Power Syst.*, Vol. 13, No. 2, pp. 401-407.
10. Jang, G., Vittal, V. & Klimann, W. (1998). Effect of nonlinear modal interaction on control performance: Use of normal forms technique in control design, Part II: Case studies. *IEEE Trans. Power Syst.*, Vol. 13, No. 2, pp. 408-413.
11. Thapar, J., Vittal, V., Kliemann, W. & Foad, A. A. (1998). Application of the normal form of vector fields to predict inter-area separation in power systems. *IEEE Trans. Power Syst.*, Vol. 2, No. 2, pp. 844-850.
12. Shanechi, H. M., Pariz, N. & Vaahedi, E. (2003). General nonlinear modal representation of large scale power systems. *IEEE Trans. Power Syst.*, Vol. 18, No. 3, pp.1103-1109.
13. Pariz, N., Shanechi, H. M. & Vaahedi, E. (2003). Explaining and validating stressed power systems behavior using modal series. *IEEE Trans. Power Syst.*, Vol. 18, No. 3, pp. 778-785.
14. Zou, Z. Y., Jiang, Q. Y., Cao, Y. J. & Wang, H. F. (2005). Application of the Normal Forms to analyze the interactions among the multiple-control channel of UPFC. *Int. J. Electric Power Energy Syst.*, Vol. 27, No. 8, pp. 584-593.
15. Soltani, S., Pariz, N. & Gazi, R. (2009). Extending the perturbation technique to the modal representation of nonlinear systems. *Elect. Pow. Syst. Res.*, Vol. 79, No. 8, pp. 1209-1215.
16. Messina, A. R. & Barocio, E. (2003). Nonlinear analysis of inter-area oscillations: Effect of SVC voltage support. *Elect. Pow. Syst. Res.*, Vol. 64, No. 1, pp. 17-26.
17. Barocio, E. & Messina, A. R. (2003). Normal form analysis of stressed power systems: incorporation of SVC models. *Int. J. Elect. Pow. Energy Syst.*, Vol. 25, No. 1, pp. 79-90.
18. Zou, Z. Y., Jiang, Q. Y., Cao, Y. J. & Wang, H. F. (2005). Normal form analysis of interactions among multiple SVC controllers in power systems. *IEE Proc. Gener. Transm. Distrib.*, Vol. 152, No. 4, pp. 469-474.
19. Sauer, P. & Pai, M. (1998). *Power system dynamics and stability*. Prentice Hall, New Jersey.
20. Anderson, P. M. & Fouad, A. A. (1977). Power system Control and stability. Iowa, Iowa State Univ.
21. Wang, H. F. (2000). Static synchronous series compensator to damp power system oscillation. *Elect. Pow. Syst. Res.*, Vol. 54, No. 2, pp. 113-119.
22. Naghshbandy, A. (2008). Study of fault location effects on low frequency inter-area oscillations in stressed power systems. Dissertation, Iran University of science and technology, Iran.
23. Liu, S., Messina, A. R. & Vittal, V. (2005). Assessing placement of controllers and nonlinear behavior using normal form analysis. *IEEE Trans. Power Syst.*, Vol. 20, No. 3, pp. 1486-1495.
24. Wu, F. X., Wu, H., Han, Z. X. & Gan, D. Q. (2007). Validation of Power system non-linear modal analysis methods. *Elect. Pow. Syst. Res.*, Vol. 77, No. 10, pp. 1418-1424.

APPENDIX A: Data used for simulations

Data of SSSC (in p.u. except indicated): T_{SSSC}=0.01 s, k=1, X_{SCT}=0.15, C_{DC}=1, V_{dcref}=1, X_{ref}=0.12, K_P=25, K_I=200.
Data of generator and network:

1. Synchronous generator data: Table A1.
2. Transmission line data: V_{base}=230kv, S_{base}=100MVA, X_{line}=0.001p.u/km, R_{line}=0.0001p.u/km.

3. Exciter parameters: Table A2.
4. Load flow data (in p.u.) on base 100 MVA): Q_{C1}=2.551, Q_{C2}=2.543, Q_{l1}=2.50,Q_{l2}=2.50, P_{g1}=6.644, P_{g2}=6.644, P_{g4}=5, V_3=1.02∠0 (swing bus), $|V_1|$=1.02, $|V_2|$=1.02, $|V_4|$=1.02.

Table A1. Generator data (in p.u. except indicated)

Parameter	G_1	G_2	G_3	G_4
R_a	0.0025	0.0025	0.0025	0.0025
x_d	1.8	1.8	1.8	1.8
x_q	1.7	1.7	1.7	1.7
x'_d	0.3	0.3	0.3	0.3
x'_q	0.3	0.3	0.3	0.3
T'_{do} (s)	8	8	8	8
T'_{qo} (s)	0.4	0.4	0.4	0.4
H (s)	6.5	6.5	6.5	6.5
D	9	1	11	1.2
S_{base} (MV·A)	900	900	900	900

Table A2. Exciter data (in p.u.)

Generator	K_A	T_A	T_C	T_B	T_R
1	100	0.01	1	10	0.01
2	100	0.01	1	10	0.01
3	100	0.01	1	10	0.01
4	100	0.01	1	10	0.01